Calculation of cantori for Hamiltonian flows

S. R. Hudson
Princeton Plasma Physics Laboratory, P.O. Box 451, Princeton, New Jersey 08543, USA
(Received 8 June 2006; revised manuscript received 12 September 2006; published 8 November 2006)

Cantori are the invariant sets remaining after the destruction of KAM surfaces and create partial barriers to transport in chaotic regions. Cantori may be approximated by high-order periodic orbits; however, field line tracing methods for locating periodic orbits perform poorly in chaotic regions. To approximate cantori for continuous flow dynamics, high-order periodic orbits are determined by Lagrangian variational methods. The method is robust to chaos, converges quadratically, and the computational cost scales linearly with the periodicity length of the orbit. Minimizing-periodic orbits with periodicities in the tens of thousands, that closely approximate cantori, have been constructed.

DOI: 10.1103/PhysRevE.74.056203 PACS number(s): 05.45.Ac, 05.60.Cd, 47.10.Fg, 51.20.+d

I. CONTINUOUS FLOWS AND MAPPINGS

This article will give an explicit construction of cantori for $1\frac{1}{2}$-dimensional Hamiltonian systems, where the Lagrangian for the continuous-time dynamics is given. Such systems provide the simplest realization of chaos. Examples of such systems include a particle in the field of two traveling waves [1], and the dynamics of magnetic field lines in toroidal plasma confinement devices [2]. This article seeks to illustrate that, for chaotic systems, Lagrangian variational principles [3] provide a robust approach to determining the dynamics.

It is possible to reduce the dynamics of such systems to that of a mapping on a Poincaré section [4], the mapping being determined by numerical integration. It is of course much simpler if one is given the mapping directly, and the most studied realization of chaotic systems is the standard map: $f(\theta_0,\psi_0)=(\theta_1,\psi_1)$, where $\psi_1=\psi_0-k\sin(2\pi\theta_0)/2\pi$ and $\theta_1=\theta_0+\psi_1$. Models of chaotic dynamics, such as the standard map, are invaluable for understanding the generic features of chaotic systems (see the review paper by Meiss [5]); however, physical systems of practical interest most often present themselves as continuous-time systems.

Continuous time introduces additional numerical complexity. For the standard map, the mapping on the plane is determined to machine precision by a single trigonometric calculation, an addition, and a subtraction. For the continuous-time case, the mapping is obtained by numerical integration. Consider for example the fourth-order Runge-Kutta algorithm: four calculations per step h are required to obtain a single step error of $\mathcal{O}(h^5)$. To achieve a total integration error after $N\sim\mathcal{O}(h^{-1})$ steps that is comparable to machine precision, thousands of steps and tens of thousands of calculations may be required: this is impractical, considering that thousands of iterations of the map may be required, and larger integration errors must be tolerated. However, a defining property of chaos is that nearby trajectories separate exponentially at a rate given by the Lyapunov exponent. Arbitrarily small errors will grow and ultimately overwhelm the trajectory following methods for finding periodic orbits. A more sophisticated integration algorithm is required.

II. INVARIANT PHASE-SPACE STRUCTURES

The identification of invariant phase-space structures such as cantori, plays an important role in understanding the long-time behavior of dynamical systems. If the system is integrable, a continuous foliation of the three-dimensional phase space by invariant, two-dimensional surfaces exists, on which the frequency ι (winding number, or rotational transform in toroidal plasma confinement terminology) may be rational or irrational. Consequently, the behavior of the system is known for all time: in suitable coordinates, the *action* coordinate is constant, and the *angle* coordinate increases linearly with time at a rate given by the frequency [6].

The continuous foliation by invariant surfaces is broken by even just a small perturbation. The rational two-dimensional manifolds, really a continuous family of periodic orbits, are the first to be destroyed, and chains of islands will form. For each such surface, two periodic orbits will survive: the Poincaré-Birkhoff periodic orbits. These orbits are (i) the minimizing orbit, which is generically unstable and hyperbolic, and (ii) the minimax orbit, which, for small perturbation, is stable and elliptic [4,5,7,8].

Some of the irrational surfaces are also destroyed by perturbation, but the Kolmogorov-Arnold-Moser (KAM) theorem shows that many will survive [9,10]. Exactly which KAM surfaces survive for a given perturbation can be determined by Greene's residue criterion [11].

For a slightly perturbed system, a discrete selection of the KAM surfaces can be used to partition the phase space into separate regions: trajectories cannot cross the KAM surfaces. A construction of "discrete action-angle coordinates," using a finite number of KAM surfaces as coordinate surfaces, has been implemented for chaotic magnetic fields that are relevant to plasma confinement devices [12]. On these surfaces, the dynamics is again trivial, being restricted to a two-dimensional surface, where a suitable angle coordinate increases linearly. Between the KAM surfaces, the motion can be intricate and trajectories may wander seemingly randomly in phase space. However, there are invariant structures that restrict transport, even in the chaotic regions where no KAM surfaces exist.

III. CANTORI

As the perturbation passes a critical value, a KAM surface will evaporate into an invariant set, with irrational frequency,

and with an infinite sequence of "gaps" [13–15]. Each such set is called a cantorus [15]. In contrast to the KAM surfaces, the cantori are leaky: trajectories can pass through the gaps. However, depending on the system, cantori can severely restrict the transport and thus effectively partition even the chaotic regions of phase space [16].

Cantori may be labeled by their frequency, and they are approximated by high-order, minimizing-periodic orbits, where the (rational) frequency of the periodic orbits approximates the (irrational) frequency of the cantori. To locate high-order periodic orbits in chaotic regions of phase space, Lagrangian variational principles are employed [3,17]. Such methods are based on a discretization of the action integral. Hamilton's principle of stationary action is used to determine trajectories.

IV. LAGRANGIAN VARIATIONAL PRINCIPLES

Reflecting our background in toroidal plasma confinement [18], the dynamical flow we consider is that of a toroidal magnetic field, which is analogous to a $1\frac{1}{2}$-dimensional Hamiltonian system. The magnetic field lines are those particular curves $\mathcal{C}$ that are stationary curves of the action integral [19].

$$S_{\mathcal{C}} = \int_{\mathcal{C}} \mathbf{A} \cdot \boldsymbol{dl}, \tag{1}$$

where $\mathbf{A}$ is the magnetic vector potential, which is analogous to the Lagrangian.

We use a vector potential in canonical form

$$\mathbf{A} = \psi \boldsymbol{\nabla} \theta - \chi \boldsymbol{\nabla} \phi, \tag{2}$$

where $\chi(\psi, \theta, \phi)$ is the field-line Hamiltonian, and ψ, θ, and ϕ are the radial, poloidal angle, and toroidal angle coordinates, which are in turn analogous to the momentum, position, and time coordinates of Hamiltonian systems. The Hamiltonian is written in integrable plus perturbation form

$$\chi = \frac{1}{2}\psi^2 + \sum_{m,n} \chi_{m,n}(\psi)\cos(m\theta - n\phi). \tag{3}$$

This Hamiltonian is quite general, and in essence is equivalent to the two-wave model of Escande [1].

This vector potential is "stellarator symmetric," equivalent to time-reversal symmetry [20], by virtue of $\chi(-\theta,-\phi) = \chi(\theta,\phi)$. This simplifies the numerics, as the periodic orbits that must be found lie on symmetry lines and they are equal to their image under the symmetry operation [21].

Setting each of the Fréchet derivatives of the action integral Eq. (1) to zero results in the field-line equations: $\dot{\theta} = B^{\theta}/B^{\phi}$, $\dot{\psi} = B^{\psi}/B^{\phi}$.

For numerical work, the continuous curve $\mathcal{C}$ must be represented by a finite number of parameters. It is sufficient, and simplest, to use a piecewise-linear representation, $\mathcal{C}_h$. Between $\phi_i = i\Delta\phi$ and ϕ_{i+1}, the curve $\mathcal{C}_h(\phi)$ is defined $\theta = \theta_i + (\theta_{i+1} - \theta_i)(\phi - \phi_i)/\Delta\phi$, for $\Delta\phi = 2\pi q/N$, and h is shorthand for the grid resolution, $h = \Delta\phi$. The curve is restricted to be (p,q) periodic, where p and q are integers, by constraining $\theta_N = \theta_0 + 2\pi p$. The radial coordinate is identified as $\psi = \dot{\theta}(\phi)$, where the dot denotes the derivative with respect to ϕ, and is piecewise constant: $\psi_i = (\theta_{i+1} - \theta_i)/\Delta\phi$. The radial curve is discontinuous, but it is an integrable function and sufficient for the action integral to be defined.

At first, the piecewise-linear approximation seems crude, but the action integral becomes piecewise directly solvable;

$$S = \sum_i \int_{\phi_i}^{\phi_{i+1}} (\psi\dot{\theta} - \chi) d\phi = \sum_i S_i(\theta_i, \theta_{i+1}), \tag{4}$$

where

$$S_i(\theta_i, \theta_{i+1}) = \frac{1}{2}\psi_i^2 \Delta\phi + \sum_{m,n} \chi_{m,n}(\psi_i) \left. \frac{\sin(m\theta - n\phi)}{m\dot{\theta} - n} \right|_{\phi_i}^{\phi_{i+1}}. \tag{5}$$

The discretized action integral is a rapidly computable function of N-independent parameters, $\{\theta_0, \theta_1, \ldots, \theta_{N-1}\}$, and all that remains is to find stationary curves. As the grid resolution h is decreased, the piecewise-linear $\mathcal{C}_h$ curve will more closely approximate the true, smooth continuous curve $\mathcal{C}$, with the error scaling as $\mathcal{O}(h^2)$. In the following sections, typically four straight line segments per 2π are used to approximate the continuous curves.

The basis of the variational approach is to compute the line integral of the Lagrangian along a curve. It is not required to follow trajectories, and thus the approach is immune to the exponential increase of errors.

A variety of techniques can be used to find stationary curves. For example, the gradient method of Aubry may be used [22], where starting from an initial integrable guess, the trial curve is allowed to slide down the direction of the action gradient until it reaches the minimum. Following Schellnhuber *et al.* [23], we adopt a more efficient Newton method.

V. MULTIDIMENSIONAL NEWTON METHOD

We now find curves for which the action gradient is zero. The action gradient vector is $\nabla S = (\partial S/\partial\theta_1, \partial S/\partial\theta_2, \ldots)^T$, where

$$\frac{\partial S}{\partial \theta_i} = \partial_2 S_{i-1}(\theta_{i-1}, \theta_i) + \partial_1 S_i(\theta_i, \theta_{i+1}), \tag{6}$$

where $\partial_1 S_i(\theta_i, \theta_{i+1})$, $\partial_2 S_i(\theta_i, \theta_{i+1})$ denote the derivatives of $S_i(\theta_i, \theta_{i+1})$ with respect to the first and second argument, respectively. The derivative matrix of the action gradient, called the Hessian, is a cyclic, tridiagonal matrix of the second derivatives of S_i.

Time-reversal, or stellarator symmetry [20] allows two important simplifications. The first is that periodic orbits lie in symmetry lines [11,21]. A symmetry line for this Hamiltonian is $L_1 = \{(\theta,\phi): \theta = 0, \phi = 0\}$. To find a periodic orbit on this line we may set $\theta_0 = 0$. This removes a degree-of-freedom in the piecewise-linear representation of the curve, and reduces the cyclic tridiagonal matrix to a standard tridiagonal matrix. Additional symmetry lines include $L_2 = \{(\theta,\phi): \theta = \pi, \phi = 0\}$ and $L_3 = \{(\theta,\phi): \theta = 0, \phi = \pi\}$. All the

periodic orbits required for this article are found on these lines.

The second important simplification to be exploited is that the periodic orbits on these symmetry lines are identical to their reflections under the symmetry operation. For example, the curve passing through L_1 satisfies $\theta(-\phi)=-\theta(\phi)$. This entails $\theta_{N-i}=2\pi p-\theta_i$ for these periodic orbits, and this halves the number of independent parameters in the piecewise-linear representation.

A multidimensional Newton scheme for finding zeros of the action gradient can now be applied. To calculate the Newton correction to an approximate curve, it is required to invert the Hessian. Being tridiagonal, this inversion is performed in $\mathcal{O}(N)$ operations; thus, the computational cost of constructing the periodic orbits scales linearly with the periodicity length. An initial guess for the Newton iterations is obtained by tracking the periodic curves from integrability as the perturbation is increased. These techniques have been implemented, and both the minimizing and minimax periodic orbits, with periodicities in the tens of thousands, can be quickly determined even for strongly chaotic fields.

VI. APPLICATION TO MODEL HAMILTONIAN

For illustration, we consider the Hamiltonian $\chi=\frac{1}{2}\psi^2-k[\cos(2\theta-\phi)+\cos(3\theta-2\phi)]$. Here, k represents the perturbation parameter. For $k=0$, the field is integrable, with frequency profile $\iota=\psi$. For nonzero k, primary islands (level 1) form at $\iota=p_1/q_1=1/2$ and $\iota=p_2/q_2=2/3$. A smaller, secondary island (level 2) will form at the mediant of these rationals, $\iota=p_3/q_3=(p_1+p_2)/(q_1+q_2)=3/5$. Additional islands (level 3) will form at 4/7, the mediant of 1/2 and 3/5, and at 5/8, the mediant of 3/5 and 2/3. By continually constructing the mediants level by level, the Farey tree of rationals is constructed [5], and island chains will form at each rational between 1/2 and 2/3.

For this Hamiltonian, for positive k, we observe that L_1 is a dominant symmetry line: along this line all island chains have a minimax periodic orbit. The odd periodicity island chains have a minimizing periodic orbit on L_2, and even periodicity chains have a minimizing periodic orbit on L_3. These may be distinguished by the eigenvalues of the full, cyclic tridiagonal Hessian: the minimax Hessian has a single negative eigenvalue, and the minimizing Hessian has only positive eigenvalues.

As the perturbation parameter k is increased, the islands will grow and at some point overlap, and the invariant curves between will be destroyed. The invariant curves that are most immune to island overlap are associated with irrationals that are furthest from low-order islands [11,24,25]. Every irrational number may be expressed as an infinite continued fraction [26],

$$\iota = a_0 + \cfrac{1}{a_1 + \cfrac{1}{a_2 + \cfrac{1}{a_3 + \cdots}}} = [a_0, a_1, a_2, a_3, \ldots], \qquad (7)$$

where the integers a_j are called the partial quotients. By truncating at the jth partial quotient, a rational approximation

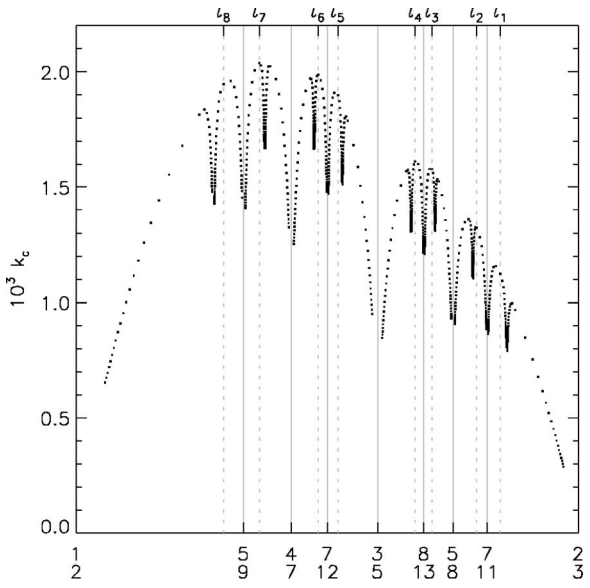

FIG. 1. Critical perturbation, k_c, for sequences of noble irrationals converging to low-order rationals.

$p_j/q_j=[a_0,a_1,a_2,\ldots,a_j]$ (called the jth convergent) to the irrational is obtained. The convergents form a sequence of consecutively better approximates. Consequently, the minimizing periodic orbits of the convergents form a sequence of consecutively better approximations to a given cantori. Irrationals with continued fraction representations terminating in infinitely many 1's, $[a_0,\ldots,a_j,1^\infty]$, are called noble irrationals. KAM surfaces with noble frequency are typically the most robust to chaos [11], and the cantori with noble frequency are often the most severe barriers to transport [27].

The critical function $k_c(\iota)$, shown in Fig. 1, is defined as the value of k at which a given invariant surface, with frequency ι, is destroyed. Rational surfaces are destroyed for $k\neq 0$, so $k_c(\iota)=0$ for every rational $\iota\in[\frac{1}{2},\frac{2}{3}]$. To compute the critical perturbation for irrational frequency, Greene's residue criterion is applied [11]. The residue, which is related to the stability of the periodic orbits, may be calculated for continuous-time systems by field line following Ref. [12], a possible task for fields not too chaotic; alternatively, it is related to the determinant of the Hessian [8]. To construct Fig. 1, the critical k for irrationals of the form $[a_0,a_1,a_2,.,a_j,n,1^\infty]$, where the a's are integers selected to give the six levels of the Farey tree spanned by 1/2 and 2/3, and $n=1,2,\ldots$, is computed. Such irrationals are noble, and the sequences converge to the rationals $[a_0,a_1,a_2,\ldots,a_j]$ as n increases: e.g., $[0,1,1,n,1^\infty]$ converges to 1/2 as $n\to\infty$. Numerically, the critical k for irrational ι is approximated by the value of k for which the residue of the tenth convergent to ι is equal to 0.25, and the required periodic orbits are found by field-line tracing along the L_1 symmetry line.

The critical function shows which irrationals are the most robust to chaos. In this case, the $[0,1,1,3,1^\infty]$ KAM surface appears to have the maximum critical k, $k_c=2.039\times10^{-3}$. For k slightly greater than this value, the $[0,1,1,3,1^\infty]$ cantori is likely to be the most important barrier to transport.

To illustrate the properties of the cantori, a set of irrationals is selected in Table. I. These are chosen to be the most

TABLE I. Selected irrationals and critical k.

Continued fraction	ι	k_c
ι_1: $[0,1,1,1,3,1,1^\infty]$	0.64073460…	1.12298
ι_2: $[0,1,1,1,2,1,1^\infty]$	0.63283980…	1.32301
ι_3: $[0,1,1,1,1,1,1^\infty]$	0.61803398…	1.57853
ι_4: $[0,1,1,1,1,2,1^\infty]$	0.61242994…	1.61074
ι_5: $[0,1,1,2,2,1,1^\infty]$	0.58674633…	1.89824
ι_6: $[0,1,1,2,1,1,1^\infty]$	0.58017872…	1.98989
ι_7: $[0,1,1,3,1,1,1^\infty]$	0.56070858…	2.03936
ι_8: $[0,1,1,4,1,1,1^\infty]$	0.54884688…	1.94805

noble irrationals between the rationals comprising the first five levels of the Farey tree: $\frac{1}{2}$, $\frac{5}{9}$, $\frac{4}{7}$, $\frac{7}{12}$, $\frac{3}{5}$, $\frac{8}{13}$, $\frac{5}{8}$, $\frac{7}{11}$, and $\frac{2}{3}$. Also given in Table. I is the critical k for each.

Cantori for the selected irrationals are shown in Fig. 2 for $k=2.10\times10^{-3}$, a value slightly greater than the maximum k_c. The cantori were approximated in the minimizing-periodic orbits with periodicities given by the 22nd convergent of each irrational (Table II).

Also shown in Fig. 2 are some low-order periodic orbits (minimizing orbits are shown with a $\times$ and the minimax are shown with a $\square$). As can be seen, the gaps in the cantori are related to the structure of the nearby periodic orbits.

To give a graphical illustration of the effect of cantori on field-line transport, field lines slightly perturbed along the

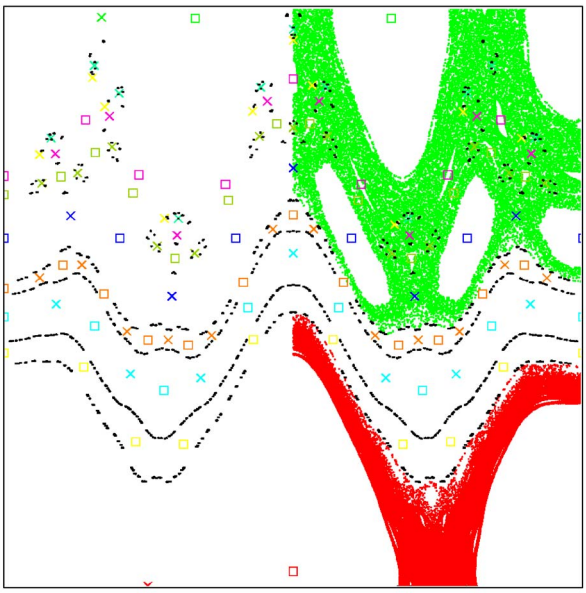

FIG. 2. (Color online) Poincaré plot showing cantori (black dots), low-order periodic orbits (minimizing $\times$, minimax $\square$), and 100 000 iterations of trajectories starting from near the $\frac{1}{2}$ and $\frac{2}{3}$ unstable periodic orbits (shown on the right side only). The horizontal θ axis extends from $[0,2\pi]$, and is symmetric about $\theta=\pi$, and the vertical ψ axis extends from $[\frac{1}{2},\frac{2}{3}]$. The perturbation parameter is $k=2.10\times10^{-3}$.

TABLE II. 22nd convergents and flux.

ι_1	(21282, 33215)	4.16×10^{-4}
ι_2	(16114, 25463)	2.60×10^{-4}
ι_3	(10946, 17711)	8.15×10^{-5}
ι_4	(15737, 25696)	6.77×10^{-5}
ι_5	(22879, 38993)	3.89×10^{-6}
ι_6	(15127, 26073)	6.05×10^{-7}
ι_7	(19308, 34435)	9.00×10^{-8}
ι_8	(23489, 42797)	1.78×10^{-6}

unstable manifolds of the $\frac{1}{2}$ and $\frac{2}{3}$ orbits are followed for 100 000 iterations. At this value of k, some of the cantori are supercritical, i.e., k is significantly greater than k_c. The supercritical cantori have little effect on transport. In the near-critical case, the cantori appear to lie on curves (with holes). These cantori play the greatest role in restricting transport, and near-critical cantori hug the boundaries of the red and green regions.

The effect of cantori on radial transport can be quantified. First, the flux across a rational island chain $\Phi_{p/q}$ is computed by constructing a surface containing the minimizing X and minimax O orbits: the flux is then simply the difference in action between these orbits, $\Phi_{p/q}=S_O-S_X$ [5,27]. The flux through the island chains, with periodicities comprising the first ten levels of the Farey tree spanned by 1/2 and 2/3, is shown in Fig. 3. This figure is similar to Fig. 56 of Meiss [5]. The flux through a cantorus is given by the limit of the flux through the convergent island chains Φ_{p_j/q_j} as the degree j of convergent increases. For the cantori shown in Fig. 2, for $k=2.10\times10^{-3}$, the limiting flux is given in Table. I.

For a KAM surface, where $k<k_c$, the flux is zero. For the near-critical case, k slightly greater than k_c, the flux is expected to satisfy the scaling given for the standard map

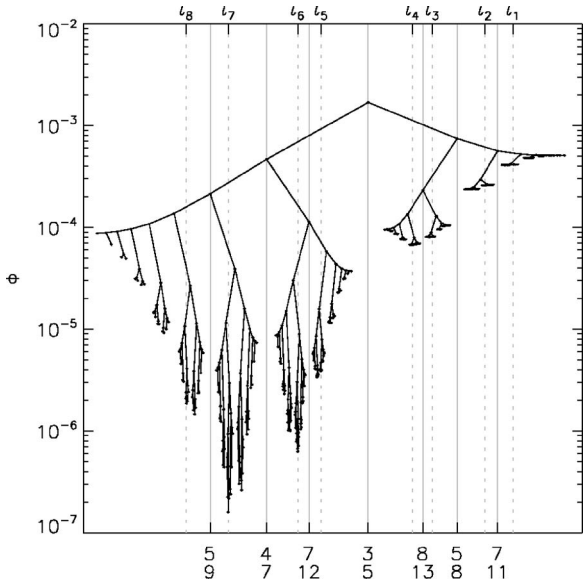

FIG. 3. Flux $\Phi_{p/q}$ against periodicity $\iota=p/q$, up to the first ten levels of the Farey tree, for $k=2.10\times10^{-3}$.

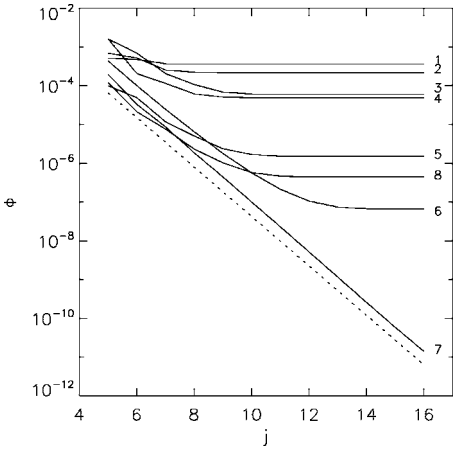

FIG. 4. Flux Φ_{p_j/q_j} against degree of convergent approximation j for each of the selected cantori, for $k=2.04\times10^{-3}$. The dashed line satisfies $\Phi=C\xi^j$ for $\xi=4.339$.

$\Phi_{p_j/q_j}=C\xi^j$, where C is a constant and $\xi\approx4.339$ [27]. The dependence of the flux Φ_{p_j/q_j} on the degree j of convergent approximation is shown in Fig. 4, for $k=2.04\times10^{-3}$, a value slightly greater than the critical k for the $[0,1,1,3,1^\infty]$ cantorus. The near-critical scaling is confirmed for the convergents of the $[0,1,1,3,1^\infty]$ cantorus.

For the supercritical cantori, the convergence with respect to j is rapid, so that quite low-order convergents give an accurate estimate of the limiting flux. A detailed investigation of the local scaling of the flux for standard like maps has been performed by Buric and Todorovic [28], and similar results are expected here.

To give a graphical illustration that the approximating minimizing-periodic orbits approximate the selected cantori, the minimizing-periodic orbits of the $[0,1,1,3,1^\infty]$ convergents are shown in Fig. 5, for $k=2.10\times10^{-3}$. The gap structure of the approximating, minimizing-periodic orbits has converged, as is clearly visible in this figure.

Finally, the error associated with a piecewise-linear approximation to a smooth curve is expected to satisfy $E(h)\sim\alpha h^2$, for some constant α and small enough h. Defining the error $E(h)$ as the root mean square of the difference between the curve $\mathcal{C}_h(\phi)$ and the curve of higher resolution $\mathcal{C}_{h/2}(\phi)$, calculated at the midpoints of the $\mathcal{C}_h$ grid $\phi=(i+\frac{1}{2})h$, it is confirmed by Fig. 6, that the error scales as expected. For this plot, the selected cantori, at the perturbation $k=2.10\times10^{-3}$, are each approximated by the 15th convergent: $\iota_1\approx733/1144$, $\iota_2\approx555/877$, $\iota_3\approx377/610$, $\iota_4\approx542/885$, $\iota_5\approx788/1343$, $\iota_6\approx521/898$, $\iota_7\approx665/1186$, and $\iota_8\approx809/1474$. Even for the supercritical cantori, the piecewise-linear representation is satisfactory. This is not surprising as the cantori remain smooth, continuous-integral curves of the continuous-time flow.

VII. DISCUSSION

We have presented a method for locating periodic orbits for continuous-flow dynamics that (i) because of the variational formulation, is robust to chaos, (ii) converges quadratically by virtue of Newton's method, and (iii) for which the computational cost scales with the length of the periodic orbit. Periodic orbits in the tens of thousands have been constructed for a strongly chaotic field. These orbits are sufficient to approximate the cantori.

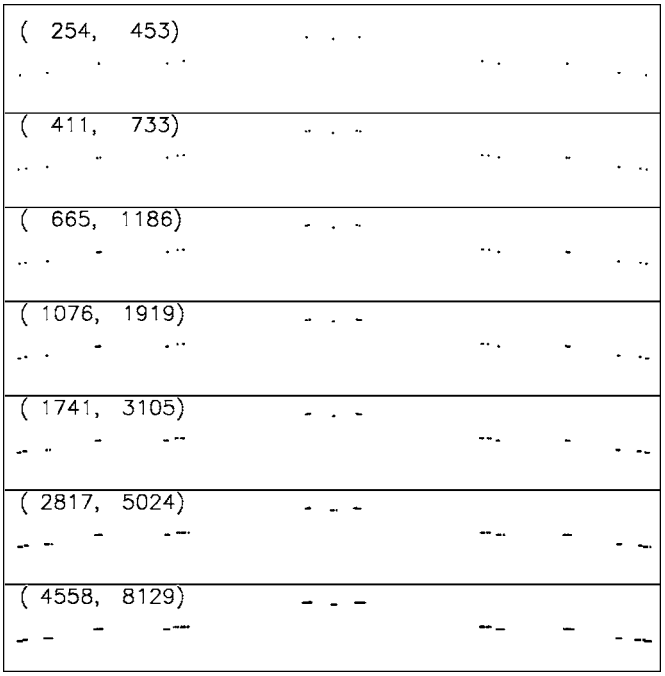

FIG. 5. Convergent minimizing-periodic orbits to the $[0,1,1,3,1^\infty]$ cantori, for the perturbation $k=2.10\times10^{-3}$. The horizontal θ range and vertical ψ range for each plot are [3.1315927, 3.1515927] and [0.5863, 0.5867], respectively.

The method is general, but the primary motivation for this work is to examine in detail the effect of cantori on toroidally confined plasmas. Toroidal confinement devices, particularly stellarators, will in general possess regions with chaotic magnetic fields, though every attempt is made to eliminate islands and the associated chaos [29]. Because of

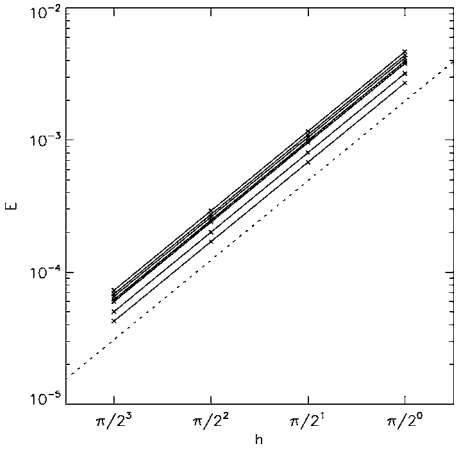

FIG. 6. Piecewise-linear approximation error against grid resolution. The dashed line has a gradient equal to 2.

the large parallel transport coefficients, the structure of the magnetic field dominates various physical mechanisms, such as heat and particle transport, and pressure relaxation, and thus it is quite likely that cantori will have an impact on numerical algorithms that seek to model these effects.

ACKNOWLEDGMENTS

This work was supported in part by U.S. Department of Energy Contract No. DE-AC02-76CH03073 and Grant No. DE-FG02-99ER54546.

[1] D. F. Escande, Phys. Scr., T **2**, 126 (1982).
[2] W. D. D'haeseleer, W. N. G. Hitchon, J. D. Callen, and J. L. Shohet, *Flux Coordinates and Magnetic Field Structure* (Springer, Berlin, 1991).
[3] A. Lew, J. E. Marsden, M. Ortiz, and M. West, Int. J. Numer. Methods Eng. **60**, 153 (2004).
[4] A. J. Lichtenberg and M. A. Lieberman, *Regular and Chaotic Dynamics*, 2nd ed. (Springer-Verlag, New York, 1992).
[5] J. D. Meiss, Rev. Mod. Phys. **64**, 795 (1992).
[6] H. Goldstein, *Classical Mechanics*, 2nd ed. (Addison-Wesley, Massachusetts, 1980).
[7] D. K. Arrowsmith and C. M. Place, *An Introduction to Dynamical Systems* (Cambridge University Press, Cambridge, U.K., 1991).
[8] R. S. MacKay and J. D. Meiss, Phys. Lett. **98A**, 92 (1983).
[9] J. Moser, *Stable and Random Motions* (Princeton University Press, Princeton, N.J., 1973).
[10] V. I. Arnold, *Mathematical Methods of Classical Mechanics* (Springer-Verlag Press, New York, 1978).
[11] J. M. Greene, J. Math. Phys. **20**, 1183 (1979).
[12] S. R. Hudson, Phys. Plasmas **11**, 677 (2004).
[13] S. Aubry, Physica D **7**, 240 (1983).
[14] J. N. Mather, Topology **21**, 457 (1982).
[15] I. C. Percival, in *Variational Principles for Invariant Tori and Cantori*, edited by M. Month and J. C. Herra, AIP Conf. Proc. No. 57 (AIP, New York, 1979).
[16] R. S. MacKay, J. D. Meiss, and I. C. Percival, Phys. Rev. Lett. **52**, 697 (1984).
[17] S. R. Hudson and R. L. Dewar, J. Plasma Phys. **56**, 361 (1996).
[18] A. H. Boozer, Rev. Mod. Phys. **76**, 1071 (2004).
[19] J. R. Cary and R. G. Littlejohn, Ann. Phys. **151**, 1 (1983).
[20] R. L. Dewar and S. R. Hudson, Physica D **112**, 275 (1997).
[21] H. Kook and J. D. Meiss, Physica D **1**, 65 (1989).
[22] S. Aubry and P. Y. Le Daeron, Physica D **13**, 381 (1983).
[23] H. J. Schellnhuber, H. Urbschat, and A. Block, Phys. Rev. A **33**, 2856 (1986).
[24] J. M. Greene, R. S. MacKay, and J. Stark, Physica D **21**, 267 (1986).
[25] R. S. MacKay and J. Stark, Nonlinearity **5**, 867 (1992).
[26] I. Niven, *Irrational Numbers* (The Mathematical Association of America, 1956).
[27] R. S. MacKay, J. D. Meiss, and I. C. Percival, Physica D **13**, 55 (1984).
[28] N. Buric and K. Todorovic, Phys. Rev. E **66**, 046221 (2002).
[29] S. R. Hudson, D. A. Monticello, A. Reiman, A. H. Boozer, D. J. Strickler, S. P. Hirshman, and M. C. Zarnstorff, Phys. Rev. Lett. **89**, 275003 (2002).